Development of a damage viscoelastic model using the thick level set approach to fracture: 1D modeling and comparison to uniaxial tension stress tests on bituminous specimens

Benjamin Shiferaw, Olivier Chupin, Jean Michel Piau, Nicolas Moes

Development of a damage viscoelastic model using the thick level set approach to fracture: 1D modeling and comparison to uniaxial tension stress tests on bituminous specimens

Benjamin Shiferaw[1], Olivier Chupin[1*], Jean-Michel Piau[1] and Nicolas Moës[2,3]

[1] MAST-LAMES, Univ Gustave Eiffel, IFSTTAR, F-44344 Bouguenais, France
[2] GeM Institute, Ecole Centrale de Nantes, France
[3] Institut Universitaire de France
[*] Corresponding author

Abstract

The present paper deals with the development of a mechanical model coupling damage and viscoelasticity for applications related to fracture in bituminous materials and structures. The behavior of these materials is highly thermo-sensitive and depends on the loading rate. Currently, there is no consensus on a modeling approach able to capture their behavior to fracture for a wide range of temperature and loading conditions. This is an objective of the model developed in this paper. Prior to damage initiation, this one is assumed purely viscoelastic and relies on the spectral decomposition of the creep function and the time-temperature superposition principle for the thermal dependency. Damage is later incorporated in the model on the basis of the concept of effective stress and a damage evolution law postulated at the local level, then regularized according to the thick level set (TLS) approach for the purpose of structural computations. This is the first modeling combining the TLS approach and viscoelasticity. This novel model is implemented in a numerical program in 1D and applied to the simulation of uniaxial tensile stress tests (UTST) carried out on a bituminous material at several temperatures and a given monotonic displacement rate. By defining the critical energy release rate as a function of temperature in the model, the numerical simulations compare favorably with the experimental results for all the tested temperatures, proving the capacity of this model to capture brittleness/ductileness of the bituminous samples depending on temperature. Based on the test simulations, other features of the model are also discussed.

Keywords: thermo-viscoelasticity, damage, Thick Level Set approach (TLS), Poynting-Thomson model, Generalized Kelvin-Voigt model, uniaxial tension stress test, bituminous mixtures.

Nomenclature of the main or recurrent quantities

$\dot{(\ )}$	Rate quantity
$\bar{(\ )}$	Nonlocal TLS quantity
$()_{ND}$	Quantity related to the undamaged material
$()_{D}$	Quantity related to the damaged material
$()^{t}$	Quantity at time t
$()^{t+dt}$	Quantity at time $t+dt$
$\partial/\partial t$	Time partial derivative
i	Imaginary unit
$\omega\ (s^{-1})$	Pulsation
$t\ (s)$	Time
$\theta\ (°C)$	Temperature of the material
$\theta_{ref}\ (°C)$	Reference temperature
$T\ (\Delta°C)$	Temperature difference with respect to θ_{ref} : $T=\theta-\theta_{ref}$
$E_H^*\ (Pa)$	Complex modulus of the Huet model (viscoelastic)
$E_\infty\ (Pa)$	Instantaneous modulus of the Huet model
h, k, δ	Constants of the Huet model

$F_H\ (Pa^{-1})$	Creep function of the Huet model
Γ	Gamma function
$\tau\ (s)$	Time response coefficient (viscoelasticity)
a_T	Shift factor (time-temperature superposition principle)
TLS	Thick Level Set approach
PT	Poynting-Thomson rheological law
DGKV	Damageable Generalized Kelvin-Voigt model
DGKV-TLS	Nonlocal DGKV model derived according to the TLS approach
$\sigma\ (Pa)$	Total uniaxial stress
ε	Total uniaxial strain of the DGKV or PT rheological law
ε_0	Strain in the isolated spring of the DGKV or PT rheological law
ε_i	Strain in the ith Kelvin-Voigt unit of the DGKV model (ε_1 for the PT model)
$E_0\ (Pa)$	Young modulus of the isolated spring of the DGKV or PT rheological law
$\tau_i\ (s)$	Characteristic time of the ith Kelvin-Voigt unit of the DGKV model (τ_1 for the PT model)
$E_i\ (Pa)$	Young modulus time of the ith Kelvin-Voigt unit of the DGKV model ($E_1$for the PT model)
$\eta_i\ (Pa.s)$	Viscosity of the ith Kelvin-Voigt unit of the DGKV model (η_1 for the PT model)
D	Damage variable
$\psi\ (J/kg)$	Specific density of the Helmholtz free energy
$\mathbb{T}\ (K)$	Absolute temperature
$\mathbb{T}_{ref}\ (K)$	Absolute reference temperature
$C\ (J/K/kg)$	Heat capacity
$\rho\ (kg/m^3)$	Density
$\Phi_{int}\ (W/m^3)$	Intrinsic dissipation potential
$Y\ (Pa)$	Energy release rate density
$Y_c\ (Pa)$	Critical energy release rate
$H(D)$	Softening function
$H'(D)$	Derivative with respect to D of the softening function $H(D)$
α, β	Constant of the softening function $H(D)$
$f\ (Pa)$	Damage criterion
$\sigma_{\eta_1}\ (Pa)$	Stress in the dashpot of the PT model
φ^{*Y}	Damage-based dissipation potential
$\partial\varphi^{*Y}$	Subderivative of the convex function φ^{*Y}
$\sigma_{\dot{\varepsilon}\to 0}^{ini}\ (Pa)$	Stress at initialization of damage for the PT model and for $\dot{\varepsilon} \to 0^+$
$\sigma_{\dot{\varepsilon}\to 0}^{rup}\ (Pa)$	Stress at rupture for the PT model and for $\dot{\varepsilon} \to 0^+$
$\sigma_{\dot{\varepsilon}\to \infty}^{ini}\ (Pa)$	Stress at initialization of damage for the PT model and for $\dot{\varepsilon} \to \infty$
$\sigma_{\dot{\varepsilon}\to \infty}^{rup}\ (Pa)$	Stress at rupture for the PT model and for $\dot{\varepsilon} \to \infty$
$\dot{U}\ (m/s)$	Imposed displacement rate (>0) of the bar problem
$l(t)\ (m)$	Damage front location at time t
$l_c\ (m)$	Critical length of the nonlocal damage model
$L\ (m)$	Length of the bar in the 1D problem
$\varphi(x,t)$	Level set function
WLF	Williams-Landel-Ferry law
C_1, C_2	Coefficients of the WLF law
$FU\ (J)$	Work of external forces (the bar problem)
$W_{VE}\ (J)$	Energy dissipated by viscoelasticity (the bar problem)
$W_D\ (J)$	Energy dissipated by damage (the bar problem)
$W_{dissipated}\ (J)$	Total energy dissipated (the bar problem)

Introduction

The study of fracture in viscoelastic media started in the early 1960's by Max L. Williams who extended Griffith's work to the domain of linear viscoelasticity [1]. The simple case of a three-dimensional medium including a spherical flaw loaded by hydrostatic tension was considered. Based on this study, cracking in viscoelastic material was found to depend on the loading history [2]. This research was then used by many authors to solve engineering problems, especially related to the failure of polymers and elastomers. This is also of interest in the field of pavement mechanics that involves bituminous materials which are also viscoelastic and sensitive to temperature. Indeed, fracture process in bituminous materials occurs in many issues related in particular to durability and maintenance operations in pavements. These can imply either fracture by fatigue (*e.g.* road traffic) or fracture at low number of loading cycles or under monotonous loading (*e.g.* extreme climatic conditions). In this context, the purpose of this paper is to develop a modeling approach to fracture in bituminous materials and structures under monotonous loading that can be applied to a large range of loading rate and temperature conditions. A recent state-of-the-art on the mechanisms of cracking in asphalt materials [3] has revealed that no consensus exits yet on the way to account for this problematic. Nonetheless, numerous papers can be found in the literature about the modeling of cracking in these materials which is often addressed through different approaches depending in particular on temperature under consideration.

At freezing temperature, the linear elastic fracture mechanics is frequently used because the response of bituminous materials can be considered as linear elastic. In order to account for a fracture process zone where micro-cracks develop and coalesce leading locally to softening of the material, the cohesive zone model (CZM) was also introduced in the field of pavement mechanics [4][5][6][7]. Since this early research involving CZM, progress has been made to account for the viscoelastic behavior of bituminous materials that becomes more pronounced at higher temperature [8]. More recently, an intrinsic CZM-based approach with deformation rate effect coupled with a linear viscoelastic behavior in the bulk of the material was developed [9]. This approach was able to capture the experimental response of specimens tested at ambient controlled temperature and for different loading rates. This study emphasized on the importance of considering the deformation rate effect in both the bulk and the fracture process zone of CZM approaches to well represent experimental data. Note that this technique and more generally fracture mechanics benefit from the development of the extended finite element method (XFEM) for taking into account geometrical discontinuities in finite element meshes [10]. This technique has also been applied to fracture in viscoelasticity [11], [12].

Apart from these crack-based models, another way to simulate the failure of structures is to consider the continuum damage approach as an ingredient of the constitutive behavior of the materials. As well-known, these models require regularization to avoid the occurrence of spurious localization in numerical simulations. Several regularization techniques can be distinguished nowadays: the non-local integral formulation (*e.g.* [13] and [14] in the context of bituminous materials), the high-order gradient formulation [15], the phase-field approach [16] ([17] for fracture in viscoelastic solids), and the Thick Level Set (TLS) approach [18], [19]. The latter is considered in this paper. The TLS approach is a non-local model that offers the possibility of a smooth transition from damage to the development of cracks. Combined with XFEM this approach can handle complicated crack topology such as branching and merging in 2D and 3D [20]. This approach was first developed in linear elasticity. The purpose here is to propose an extension to viscoelastic materials. At this stage, the development is restricted to the 1D case to assess the capability of the model to simulate fracture in bituminous materials, keeping with a quite simple numerical implementation that does not require the use of the finite element framework. The developed model is applied to the modeling of uniaxial tensile stress tests (UTST) and evaluated by comparison to experimental results stemming from bituminous specimens tested at different temperatures. The result of this study can also be viewed as a reference solution that could be used in the future to validate the implementation of this viscoelastic TLS model in finite element numerical programs in 2D or 3D, involving more complex solving strategies.

The paper is outlined as follows. After a preamble about creep function for asphalt materials and the spectral decomposition, the development of the local 1D constitutive law based on the concept of effective stress and coupling damage and viscoelasticity is presented. Then, the problem of a viscoelastic bar subjected to direct tension until rupture is formulated using the TLS approach. A space discretization and time implicit scheme involving Newton iterations are utilized to solve the resulting nonlinear transient equations. The solution is implemented in a numerical program used to simulate the UTST tests mentioned above. The ability of the model to capture the experimental response of the bituminous specimens at different temperatures is evaluated. Finally, some other specific features of the model are discussed.

1. Creep function for asphalt concrete material and spectral decomposition

1.1 The Huet constitutive law

The viscoelastic behavior of asphalt concrete materials is well represented by the Huet constitutive law which is largely described in the literature [21][22]. This rheological model is composed of a series of two parabolic dashpots and a linear spring. The equations for its complex modulus E_H^* and creep function F_H are given by:

$$E_H^*(\omega,\theta) = \frac{E_\infty}{1+(i\omega\tau(T))^{-h}+\delta(i\omega\tau(T))^{-k}} \quad (1)$$

$$F_H(t,\theta) = \frac{1}{E_\infty}\left(1+\frac{\left(\frac{t}{\tau(T)}\right)^h}{\Gamma(h+1)}+\frac{\delta\left(\frac{t}{\tau(T)}\right)^k}{\Gamma(k+1)}\right) \quad (2)$$

with ω = pulsation (s^{-1}), t = time (s), T = difference between the considered temperature θ ($°C$) and a reference one θ_{ref}, E_∞ = instantaneous modulus (Pa), h, k = exponents of the parabolic dashpots ($0 < h < k < 1$), δ = weighting coefficient ($\delta > 0$), and Γ = Gamma function. These equations account for the sensitivity to temperature which is considered to follow the time-temperature superposition principle. The time response coefficient $\tau(T)$ is expressed as: $\tau(T) = a_T(T)\tau_{ref}$, where a_T is the shift factor decreasing with temperature. The creep function is calibrated and used in the numerical example below (section 4).

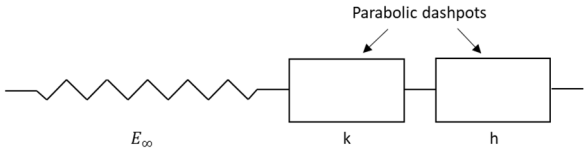

Fig. 1. The Huet rheological model

1.2 Spectral decomposition of creep functions

The upcoming developments will be based on the spectral decomposition of creep functions and in particular on that of the Huet model. The spectral decomposition consists in representing the rheological behavior of a viscoelastic material as a series of Kelvin-Voigt elements. These series can be derived from the creep function and can be continuous (integral shape) or discrete (with a summation index). In the latter case the series can be infinite or finite. In numerical applications, finite series with a limited number of Kelvin-Voigt models are often used as an approximate of the actual behavior in order to handle only a reasonable number of internal state variables. Such a strategy is adopted in this paper.

This led us at first to develop a damage model based on the Poynting-Thomson (PT) rheological law (or solid linear standard model) that can be viewed as associating instantaneous elasticity with one Kelvin-Voigt element (Fig. 2). Then, a more general damage model based on a spectral series composed of N_{KV} elements of Kelvin-Voigt and a spring (instantaneous elasticity) was easily derived from that relying on the PT model. This more sophisticated model obtained from the Huet model decomposition is obviously more appropriate to reproduce damage developing in asphalt concrete materials.

Note that the time-temperature superposition principle is now reflected by a dashpot viscosity taken as proportional to the ~~shift factor~~ time response coefficient $\tau(\theta)$ for each Kelvin-Voigt element.

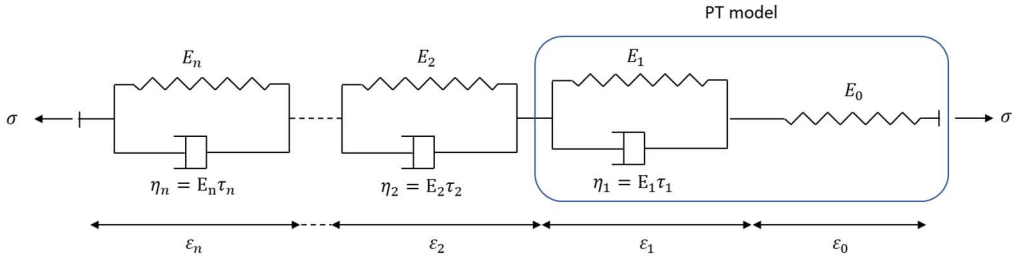

Fig. 2. The generalized Kelvin-Voigt model with n elements

2. Development of a local viscoelastic damage model in 1D

2.1 Equations of the PT constitutive law

The set of equations that describe the PT model is as follows:

$$\sigma = E_0 \varepsilon_0 \tag{3}$$

$$\sigma = E_1 \varepsilon_1 + \eta_1 \dot{\varepsilon_1} = E_1(\varepsilon_1 + \tau_1 \dot{\varepsilon_1}) \tag{4}$$

$$\varepsilon = \varepsilon_1 + \varepsilon_0 \tag{5}$$

where σ is the total stress and ε the total strain in the PT model. The viscosity η_1 of the model can be expressed as a function of the characteristic time τ_1 and the Young modulus E_1 such as: $\eta_1 = E_1 \tau_1$. For a thermo-sensitive model that satisfies the time-temperature superposition principle, τ_1 depends on temperature but E_0 and E_1 do not. For the generalized discrete model composed of several Kelvin-Voigt elements addressed further, the τ_i of each dashpot is affected by the same function $\tau(T)$ such as: $\tau_i(T) = \alpha_i \tau(T)$, with α_i a positive scalar.

Combining the equations above makes it possible to eliminate the internal strain variables ε_0 and ε_1:

$$\sigma = \frac{E_0 E_1}{(E_0+E_1)} \varepsilon + \frac{E_0 \eta_1}{(E_0+E_1)} \dot{\varepsilon} - \frac{\eta_1}{(E_0+E_1)} \dot{\sigma} \tag{6}$$

or equivalently:

$$\varepsilon(t) = \left(\frac{1}{E_0} + \frac{1}{E_1 + \eta_1 \frac{\partial}{\partial t}} \right) \sigma(t) \tag{7}$$

in which the differential operator $\left(\frac{\partial}{\partial t}\right)$ is treated as an algebraic entity [23].

2.2 Introducing damage in the viscoelastic PT model

The effective stress principle is adopted to introduce local damage in the viscoelastic PT model. This consists in replacing in the previous constitutive law σ by the effective stress $\tilde{\sigma}$ defined in 1D as:

$$\tilde{\sigma} = \sigma/(1-D) \tag{8}$$

D is the scalar damage variable equal to 0 for the sound material and to 1 for the fully damaged state ($0 \leq D \leq 1$). The resulting model is equivalent to the PT viscoelastic model in which all the basic rheological elements are diminished by the factor $(1-D)$ (Fig. 3).

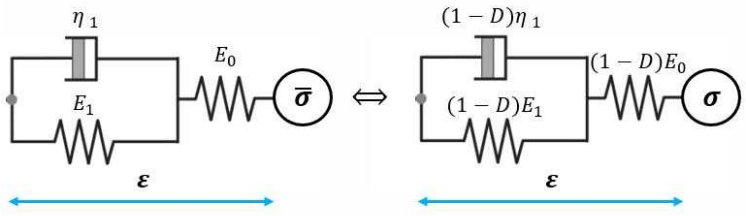

Fig. 3. Damaged PT model within the effective stress concept

The state laws now read:

$$\sigma = (1-D) E_0 \varepsilon_0 \tag{9}$$

$$\sigma = (1-D) E_1 \varepsilon_1 + (1-D) \eta_1 \dot{\varepsilon}_1 \tag{10}$$

$$\dot{\sigma} = (1-D) E_0 \, \dot{\varepsilon} - \left(\frac{E_0+E_1}{\eta_1} + \frac{\dot{D}}{1-D} \right) \sigma + (1-D) \frac{E_0 E_1}{\eta_1} \varepsilon \tag{11}$$

In order to derive the evolution model for D, let us recast these equations in the framework of thermodynamics. ε, ε_1, D and T can be defined as the state variables for the derivation of the specific density of the Helmholtz free

energy, $\psi(\varepsilon, \varepsilon_1, D, T)$. By integration of equation $\sigma = \rho\partial\psi/\partial\varepsilon$ and $\sigma_{\eta_1} = -\rho\partial\psi/\partial\varepsilon_1$, where σ_{η_1} represents the stress in the dashpot (Clausius-Duhem inequality), we can define ψ as:

$$\rho\psi(\varepsilon, \varepsilon_1, D, T) = \frac{1}{2}(1-D)[E_0(\varepsilon-\varepsilon_1)^2 + E_1\varepsilon_1^2] - \rho C\mathbb{T}\, ln(\mathbb{T}) + g(D,T) \quad (12)$$

in which $\mathbb{T} = \mathbb{T}_{ref} + T$ is the absolute temperature. The second term in the right-hand side considers the specific heat capacity of the material that contributes to the heat equation. Note that we do not consider thermal dilation in Eq. (10) which makes sense since only simulations under isothermal conditions will be performed in this paper. Besides, $g(D,T)$ is set equal to zero in the following to keep with the conventional damage theory. However, considering this term would be interesting to study self-healing mechanisms for instance, which are often mentioned regarding the behavior of bituminous materials.

The Clausius-Duhem inequality then leads to ensure positivity of the intrinsic dissipation given by:

$$\Phi_{int} = -\rho\frac{\partial\psi}{\partial\varepsilon_1}\dot{\varepsilon}_1 - \rho\frac{\partial\psi}{\partial D}\dot{D} = \sigma_{\eta_1}\dot{\varepsilon}_1 + Y\dot{D} \quad (13)$$

where $Y = -\rho\partial\psi/\partial D$ is the energy release rate density. In practice, we seek for positivity of each term separately. The first term $\sigma_{\eta_1}\dot{\varepsilon}_1$ is positive from the dashpot constitutive law since $\sigma_{\eta_1} = (1-D)\eta\dot{\varepsilon}_1$. In the present case, Y given by Eq. (14), is always positive.

$$Y = -\rho\frac{\partial\psi}{\partial D} = \frac{1}{2}[E_0(\varepsilon-\varepsilon_1)^2 + E_1\varepsilon_1^2] \quad (14)$$

Consequently, $\dot{D}$ will have to be positive in the following. To ensure this condition $\dot{D}$ will be defined as the derivative (or subderivative) of a convex function φ^{*Y} of Y (damage-based dissipation potential).

2.3 Dissipation potential and damage evolution

Here, the choice is made to use a dissipation potential of the form:

$$\varphi^{*Y}(Y, \varepsilon, \varepsilon_1, D) = +\infty \text{ if } \mathrm{Y} > \mathrm{Y_c}H(D) \text{ and } \varepsilon - \varepsilon_1 > 0$$
$$\varphi^{*Y}(Y, \varepsilon, \varepsilon_1, D) = 0 \text{ otherwise} \quad (15)$$

which is convex with respect to Y. Material parameters Y_c and $H(D)$ define a threshold for the damage criterion. Y_c is a positive scalar of same unit as stress and $H(D)$ is called the softening function. $H(D)$ is positive and verifies $H(0) = 1$. The condition on $\varepsilon - \varepsilon_1$ which is related to the sign of stress in the PT model reflects the fact that damage is assumed to occur only in traction. The evolution law defined by $\dot{D} \in \partial\varphi^{*Y}$, where $\partial\varphi^{*Y}$ is the subderivative set of φ^{*Y} with respect to Y, is equivalent to the Karush-Kuhn-Tucker conditions [24]:

$$f = Y - Y_c H(D) \leq 0,\ \dot{D} \geq 0,\ f\dot{D} = 0 \quad (16)$$

and also, to the condition:

$$\dot{D}(\varepsilon - \varepsilon_1) \geq 0 \quad (17)$$

It can be shown easily that for this model the time-temperature superposition principle is still verified during damage growth since the dissipation potential φ^{*Y} is chosen as not depending explicitly on the temperature variable. As a consequence, the stress-strain curve corresponding to a given value of temperature T' and a given strain-driven loading history $\{\varepsilon(t)\} : t \to \varepsilon(t)$ can be deduced from the stress-strain curve at T by shifting the time variable as shown in Eq. (18):

$$\sigma_{\tau'}(t, \{\varepsilon(t)\}) = \sigma_\tau\left(t\frac{\tau}{\tau'}, \left\{\varepsilon\left(t\frac{\tau'}{\tau}\right)\right\}\right) \quad (18)$$

where $\tau = \tau(T)$ and $\tau' = \tau(T')$. $\sigma_{\tau'}$ and σ_τ are the stress developing in the viscoelastic-damage model at temperature T' and T.

2.4 Response of the local damage model for low and high loading rates

In order to precise further function $H(D)$, let us address the two particular cases of loading rates $\dot{\varepsilon}$ that tend to 0^+ and $+\infty$ and considering initial stress and strain to be zero. These two cases reduce to damage elastic problems with $\sigma = (1-D)E$ where E is the modulus equal to $E = E_0E_1/(E_0+E_1)$ for $\dot{\varepsilon} \to 0^+$ and $E = E_0$ for $\dot{\varepsilon} \to +\infty$.

For $\dot{\varepsilon} \to 0^+$, the stress and the strain values at initialization of damage ($D = 0, Y = Y_c$) and at rupture ($D = 1$, $Y = H(1)Y_c$) are given by:

$$\sigma^{ini}_{\dot{\varepsilon}\to 0^+} = \sqrt{2Y_c \frac{E_0E_1}{E_0+E_1}},\ \varepsilon^{ini}_{\dot{\varepsilon}\to 0^+} = \sqrt{2Y_c \frac{E_0+E_1}{E_0E_1}} \tag{19}$$

and

$$\sigma^{rup}_{\dot{\varepsilon}\to 0^+} = 0,\ \varepsilon^{rup}_{\dot{\varepsilon}\to 0^+} = \sqrt{2H(1)Y_c \frac{E_0+E_1}{E_0E_1}} \tag{20}$$

For $\dot{\varepsilon} \to +\infty$, the stress and the strain values at initialization of damage and at rupture are given by:

$$\sigma^{ini}_{\dot{\varepsilon}\to +\infty} = \sqrt{2Y_cE_0},\ \varepsilon^{ini}_{\dot{\varepsilon}\to +\infty} = \sqrt{2Y_c \frac{1}{E_0}} \tag{21}$$

and

$$\sigma^{rup}_{\dot{\varepsilon}\to +\infty} = 0,\ \varepsilon^{rup}_{\dot{\varepsilon}\to +\infty} = \sqrt{2H(1)Y_c \frac{1}{E_0}} \tag{22}$$

One can notice that the σ^{ini} stress value for $\dot{\varepsilon} \to \infty$ is greater than that for $\dot{\varepsilon} \to 0$ and conversely for ε^{ini} and ε^{rup}. Moreover, the condition $\varepsilon^{rup} > \varepsilon^{ini}$ imposes the condition $H(1) > 1$. In both cases, the damage evolution law is obtained by time differentiation of the damage criterion $Y - H(D)Y_c = 0$ with $Y = E\varepsilon^2/2$ considering the appropriate value for E, as expressed above, depending on whether $\dot{\varepsilon} \to 0$ or $\dot{\varepsilon} \to \infty$. The constitutive law during damage growth can be expressed in terms of rates by time differentiation of $\sigma = (1-D)E\varepsilon$ and Eq. (23) still using the appropriate choice for E.

$$\dot{D} = \frac{E\varepsilon\dot{\varepsilon}}{Y_cH'(D)} \tag{23}$$

$$\dot{\sigma} = \left(1 - D - \frac{2H(D)}{H'(D)}\right)E\dot{\varepsilon} = K(D)E\dot{\varepsilon} \tag{24}$$

Eq. (23) needs $H'(D) > 0$ to ensure $\dot{D}$ to be positive. Let us consider the simple linear relationship for $K(D)$:

$$K(D) = a - bD \tag{25}$$

From Eq. (24), the softening function can be expressed as a function of K as follows:

$$H(D) = e^{\int_0^D \frac{2du}{1-K(u)-u}} \quad \text{for } D \in [0,1] \tag{26}$$

which combined with Eq. (25) leads to:

$$H(D) = (1-\beta D)^{-\alpha} \quad \text{and} \quad H'(D) = \alpha\beta(1-\beta D)^{-\alpha-1} \tag{27}$$

with $\alpha = 2/(1-b)$ and $\beta = (1-b)/(1-a)$ or reversely $a = 1 - 2/\alpha\beta$ and $b = 1 - 2/\alpha$. To meet the condition $H(1) > 1$ and $H'(D) > 0$, coefficients α and β must be of same sign. Considering positive values for α and β, Eq. (27) requires $\beta < 1$ to have $H(D)$ defined for $D \in [0,1]$. It can also be checked that conditions $\alpha > 0$ and $0 < \beta < 1$ yield $K(1) = a - b < 0$ as required at rupture. On the other hand, $K(0) = a$ can be positive or

negative depending on whether $\alpha\beta > 2$ or $\alpha\beta < 2$. For $K(0) < 0$ the stress at initialization of damage, σ^{ini}, is also the maximum value of stress of the $\sigma - \varepsilon$ curve. On the contrary, for $K(0) > 0$ the stress at damage initialization occurs prior to the peak value of the $\sigma - \varepsilon$ curve.

In the example of section 4, the values of α and β for the considered asphalt concrete material will be determined based on experimental results and the nonlocal TLS model presented further. In this case α and β will be found to check $\alpha\beta > 2$.

2.5 Extension to the Generalized Kelvin-Voight model (DGKV)

The Poynting Thomson model and the introduction of damage in this model can be easily extended to a generalized Kelvin-Voigt model whose response will be more appropriate to simulate the complex behavior of asphalt concrete materials characterized by a large spectrum of relaxation times. The extension to the generalized Kelvin-Voigt model for the purely viscoelastic response leads to the replacement of Eqs. (4) and (5) by:

$$\sigma = E_i(\varepsilon_i + \tau_i \dot{\varepsilon}_i) \tag{28}$$

$$\varepsilon = \varepsilon_0 + \sum_i \varepsilon_i \tag{29}$$

ε_i are internal variables characterizing the strain in each of the N_{KV} Kelvin-Voigt units of the generalized model. E_i and τ_i are the stiffness of the spring and the time response of the dashpot of the ith Kelvin-Voigt unit.
For the damage viscoelastic response, applying the principle of effective stress to the whole series leads to the substitution of Eqs. (10) and (14) by:

$$\sigma = (1 - D)E_i(\varepsilon_i + \tau_i \dot{\varepsilon}_i) \tag{30}$$

$$Y = \frac{1}{2}(E_0 \varepsilon_0^2 + \sum_i E_i \varepsilon_i^2) \tag{31}$$

A numerical program based on a pure implicit time discretization scheme (see Eqs (39)-(41)) was developed to compute the $\sigma - \varepsilon$ curve of this local viscoelastic damage model for function $H(D)$ given by Eq. (24) and for a constant imposed strain rate $\dot{\varepsilon}$. As an illustration of the local response of this constitutive law and for later comparison with the nonlocal model, Fig. 4 shows for several temperatures the $\sigma - \varepsilon$ curves obtained for the material parameters of the application detailed in section 4.

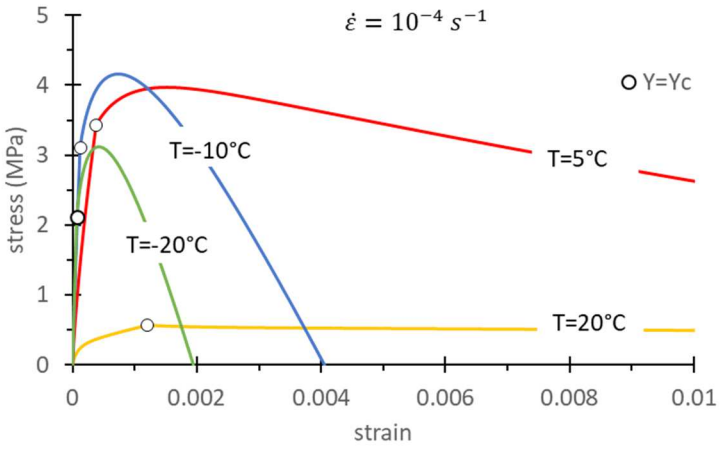

Fig. 4. Local $\sigma - \varepsilon$ curves computed at different temperatures and $\dot{\varepsilon} = cst$ for the damageable generalized Kelvin-Voigt model (material parameters shown in Tables 1 and 2 and Fig. 9). The strain at rupture for $T = 5°C$ and $T = 20°C$ (not visible for the strain scale used in the figure) are equal to approximately 3% and 10%, respectively.

3. Nonlocal TLS formulation for a viscoelastic bar under direct tension (1D) (DGKV-TLS model)

The model developed in the previous sections at the local level will now be introduced in the nonlocal framework of the Thick Level Set approach to avoid localization issues inherent to the onset and growth of damage using local models in structural problems. The TLS approach has been developed in 2D/3D already for elasticity and plasticity [18][19][20][25]. Here, the main purpose is to investigate the implementation of viscoelasticity in this approach. To this end, we consider the 1D case of a viscoelastic bar subjected to direct tension which facilitates the numerical developments needed to solve the problem. Nonetheless, the simulations can be compared to uniaxial tension tests performed on asphalt concrete specimens until rupture in order to evaluate the capability of the developed approach to reproduce the fracture behavior of thermo-sensitive viscoelastic materials. The comparison is carried out in section 4.
In this section, we first summarize the main TLS features applied to the problem of the bar in tension prior to presenting the solving algorithm.

3.1 Position of the problem and TLS approach in 1D

Let us consider a viscoelastic bar of length L clamped at the left end in $x = 0$ (Fig. 5). A positive displacement rate, $\dot{U}(L,t)$, is applied to the other end so that the bar is in extension during loading. The quasi-static equilibrium indicates that at any time of loading the stress, $\sigma(t)$, is constant along the bar. While $Y < Y_c$, the mechanical response of the bar is assumed to be purely viscoelastic and governed by the generalized Kelvin-Voigt model (Eqs. (3), (28) and (29)). Damage initiates once $Y = Y_c$ is reached. Since the response of the bar is homogeneous until $Y = Y_c$, the location of damage initialization is undetermined for this specific example without initial flaw (in contrast with real specimens which are rarely homogeneous). Consequently, the assumption is made to initiate a single damage front at the clamped end of the bar.

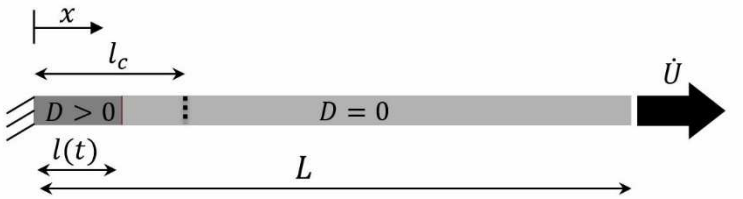

Fig. 5. Bar under direct tension and the development of a damaged zone of length $l(t)$ at time t

Damage growth in the bar is then handled by the TLS approach which is assumed here to concentrate damage in a single band of thickness $x \in [0, l(t)]$, where $l(t)$ is the damage front location separating the damaged and undamaged areas. In this band, the damage is related to the signed distance from the front location, $\varphi(x,t) = l(t) - x$, which represents here the level set function. Obviously, φ verifies the level set property $|\nabla\varphi| = 1$ and is nil at the damage front. The positive values of φ determine the damage area for which the points x inside the band play the role of the level curves. The sound area is characterized by $\varphi < 0$. The band width is limited to a maximum value l_c so-called the critical length of the nonlocal damage model. In the TLS approach, the damage distribution is determined by a smooth increasing function $D(\varphi)$ whose values vary between $D(0) = 0$ and $D(l_c) = 1$. The damage value is thus smaller than 1 for $l(t) < l_c$ and its gradient is bounded. Fig. 6 shows two examples of function $D(\varphi)$. Hereafter, the choice is made to utilize the linear function: $D(\varphi(x,t)) = (l(t) - x)/l_c$.

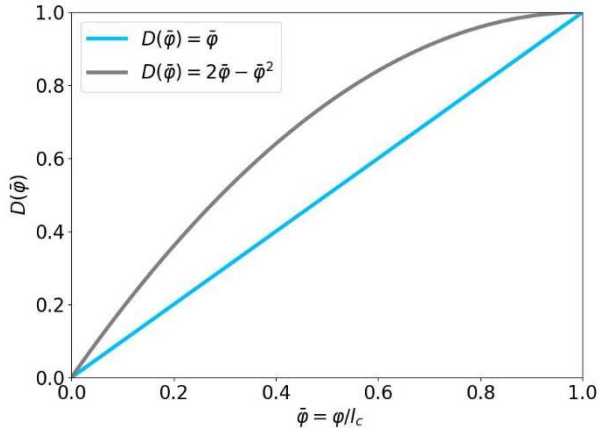

Fig. 6. Examples of function $D(\varphi)$

The evolution of damage is also governed in the TLS framework by a nonlocal expression of the Karush-Kuhn-Tucker conditions (Eq. 16):

$$\bar{f} = \bar{Y} - Y_c \bar{H}(D) \leq 0,\ \bar{\dot{D}} \geq 0,\ \bar{f}\bar{\dot{D}} = 0 \tag{32}$$

using the following averaged quantities:

$$\bar{Y} = \frac{\int_0^l Y(x)D'(x)dx}{\int_0^l D'(x)dx} = \frac{l_c}{l}\int_0^l Y(x)|D'(x)|dx \tag{33}$$

$$\bar{\dot{D}} = \frac{1}{l}\int_0^l \dot{D}dx \tag{34}$$

$$\bar{H}(D) = \frac{\int_0^l H(D)D'dx}{\int_0^l D'dx} = \frac{l_c}{l}\int_0^l H(D)|D'|dx \tag{35}$$

For the linear damage shape function $D(\varphi)$, the damage criterion function $\bar{f}$ can be taken equal to (division by l can be omitted):

$$\bar{f} = \int_0^l Y(\varphi)d\varphi - Y_c \int_0^l H(D)d\varphi \leq 0 \tag{36}$$

For the problem of the bar in tension $\bar{\dot{D}}$ is equal to $\dot{l}/l_c$. The condition $\bar{\dot{D}} > 0$ is automatically satisfied provided that the damage front continuously moves forward ($\dot{l} \geq 0$). Then, the condition $\bar{f}\bar{\dot{D}} = 0$ leads to $\bar{f} = 0$ which now drives the damage evolution in the present TLS approach.

3.2 Discretization and solving algorithm

The set of equations that governed the problem of the viscoelastic bar is solved numerically considering time and space discretization. The imposed rate of displacement, $\dot{U}(L,t) = \dot{U}(L)$, is assumed positive and constant. To ensure stability of the solution and to avoid the need for using very small timesteps, even in the presence of small characteristic times in the GKV spectrum, the time discretization of the equations is performed according to the Euler pure implicit scheme. The response of the bar is computed incrementally between two timesteps t and $t + dt$. All the quantities at time t are supposed to be known. The subscripts ND and D are used to refer to the undamaged and damaged areas in the bar.

Computation of the initial pure viscoelastic phase

The mechanical fields are uniform during this initial phase ($Y < Y_c$ in each point). The following relationship holds everywhere in the bar for each Kelvin-Voigt unit, i:

$$\dot{\varepsilon}_{i,ND} = \frac{\sigma}{E_i\tau_i} - \frac{\varepsilon_{i,ND}}{\tau_i} \tag{37}$$

Considering $\dot{\varepsilon}_{i,ND} \approx (\varepsilon_{i,ND}^{t+dt} - \varepsilon_{i,ND}^{t})/dt$, the implicit Euler scheme leads to:

$$\varepsilon_{i,ND}^{t+dt} = \frac{\tau_i\varepsilon_{i,ND}^{t}}{\tau_i+dt} + \frac{dt}{\tau_i+dt}\frac{\sigma^{t+dt}}{E_i} \tag{38}$$

On the other hand, the strain in the isolated spring of the GKV model can be expressed as $\varepsilon_{0,ND}^{t+dt} = \sigma^{t+dt}/E_0$, which combined with Eq. (29) yields the total deformation at time $t + dt$:

$$\varepsilon_{ND}^{t+dt} = \frac{\sigma^{t+dt}}{E_0} + \sum_i\left(\frac{\tau_i\varepsilon_{i,ND}^{t}}{\tau_i+dt} + \frac{dt}{\tau_i+dt}\frac{\sigma^{t+dt}}{E_i}\right) \tag{39}$$

The condition of kinematics compatibility involving the imposed displacement at the end of the bar finally leads to the determination of the stress value at time $t+dt$:

$$\sigma^{t+dt} = \frac{1}{\left(\frac{1}{E_0}+\sum_i \frac{dt}{(\tau_i+dt)E_i}\right)}\left[\bar{\varepsilon}^{t+dt} - \sum_i \frac{\tau_i \varepsilon_{i,ND}^t}{\tau_i+dt}\right] \tag{40}$$

in which $\bar{\varepsilon}^{t+dt} = \frac{U^{t+dt}(L)}{L} = \frac{t+dt}{L}\dot{U}(L)$ is the mean strain of the bar at time $t+dt$. This equation is used to compute the stress in the bar at time $t+dt$ which, once known, is used to calculate the internal strain variables $\varepsilon_{i,ND}^{t+dt}$ and Y^{t+dt} from Eq. (31).

Computation of the phase with damage growth

Similar developments can be applied after damage initiation and considering the following kinematics compatibility equation and constitutive law ε_D during the phase with damage growth:

$$\int_0^l \varepsilon_D^{t+dt} dx + (L-l)\varepsilon_{ND}^{t+dt} = U^{t+dt}(L) \tag{41}$$

with:

$$\varepsilon_D^{t+dt} = \varepsilon_{0,D}^{t+dt} + \sum_i \varepsilon_{i,D}{}^{t+dt} = \frac{\sigma^{t+dt}}{(1-D^{t+dt})E_0} + \sum_i \left[\frac{\tau_i \varepsilon_{i,D}^t}{\tau_i+dt} + \frac{dt}{\tau_i+dt}\frac{\sigma^{t+dt}}{(1-D^{t+dt})E_i}\right] \tag{42}$$

In the equations above, the front location is a function of time and the strain field in the damage band, ε_D^{t+dt}, depends on x and t.
Substituting Eqs. (39) and (42) into Eq. (41) leads to the determination of the stress value at time $t+dt$:

$$\sigma^{t+dt} = \frac{U^{t+dt}(L) - S_{12} - S_{22}}{S_{11}+S_{21}} = \frac{L\bar{\varepsilon}^{t+dt} - S_{12} - S_{22}}{S_{11}+S_{21}} \tag{43}$$

with:

$$S_{11} = \int_0^l \left(\frac{1}{(1-D^{t+dt})E_0} + \sum_i \frac{dt}{(\tau_i+dt)(1-D^{t+dt})E_i}\right) dx \tag{44}$$

$$S_{12} = \int_0^l \left(\sum_i \frac{\tau_i \varepsilon_{i,D}^t}{\tau_i+dt}\right) dx \tag{45}$$

$$S_{21} = (L-l)\left(\frac{1}{E_0} + \sum_i \frac{dt}{(\tau_i+dt)E_i}\right) \tag{46}$$

$$S_{22} = (L-l)\sum_i \frac{\tau_i \varepsilon_{i,ND}^t}{\tau_i+dt} \tag{47}$$

The solving algorithm for the phase with damage growth is based on the prescribed advancement of the damage front between two solution increments. The main unknown is then the timestep dt between the two increments. Hence, the value of damage D^{t+dt} is considered as a known quantity at time $t+dt$ that can be computed straightly from the damage front location using the relationship $D(\varphi)$. The timestep dt is sought such as the nonlocal damage criterion is nil at time $t+dt$, that is:

$$\bar{f}^{t+dt} = \int_0^l Y^{t+dt} dx - Y_c \int_0^l H(D^{t+dt}) dx = 0 \tag{48}$$

This nonlinear equation is solved using Newton's iterations which, after convergence, leads to the determination of timestep dt associated to the imposed deformation rate and to the damage front advance prescribed at the incremental level.
After initiation of damage, the maximum length, l_c, that the damage zone can reach is thus discretized into N_x elements of equal size, dx. This discretization is utilized to advance the damage front at each calculation increment ($l^{t+dt} = l^t + dx$), to compute $D^{t+dt}(x) = (l^{t+dt} - x)/l_c$ and also to calculate numerically the

integrals involved in S_{11}, S_{12} and Eq. (48). The value of damage is considered as constant by interval and equal to its value at mid-length of the interval under consideration.

Newton's iterations at the running increment $n+1$ for the determination of $t_{n+1} = t_n + dt_n$ consist in defining the iterative sequence $dt_n^{k+1} = dt_n^k + \delta t^k$ and finding at each iteration δt^k such as:

$$\langle \bar{f}'(t_n + dt_n^k; \mathcal{S}_n), \delta t^k \rangle = -\bar{f}(t_n + dt_n^k; \mathcal{S}_n) \tag{49}$$

$\mathcal{S}_n$ denotes the mechanical state at the previous increment (internal strain variables at time t in each discretization node) and notation $\langle \cdot \rangle$ is used to represent the differential of f with respect to time:

$$\bar{f}(t_n + dt_n^k + \delta t^k) - \bar{f}(t_n + dt_n^k) = \langle \bar{f}'(t_n + dt_n^k; \mathcal{S}_n), \delta t^k \rangle + \mathcal{O}(\|\delta t^k\|) \tag{50}$$

The derivative of $\bar{f}$ is computed numerically in $t_n + dt_n^k$ as follows:

$$\bar{f}'(t_n + dt_n^k; \mathcal{S}_n) = \left[\bar{f}(t_n + dt_n^k + \delta t_\epsilon; \mathcal{S}_n) - \bar{f}(t_n + dt_n^k; \mathcal{S}_n)\right]/\delta t_\epsilon \tag{51}$$

In Newton's iterations, the steps to compute $\bar{f}$ as a function of a given timestep are as follows: determination of the strain and stress components according to Eqs. (42) and (43), followed by computation of Y and $H(D)$ in each node and numerical integration of f. The algorithm developed to solve the 1D problem of the damageable viscoelastic bar under tension is implemented in a numerical program and summarized in Fig. 7.

for a given displacement $U(L,t)$ with $\dot{U}(L,t) > 0$, constant timestep dt_{VE} and input dataset

---------- (Pure viscoelastic phase) ----------

$dt = dt_{VE}$

initialization of the variables to zero

while $Y < Yc$ {

- $t \leftarrow t + dt$
- compute the mean strain at the current time : $\bar{\varepsilon}^{t+dt} = \frac{U^{t+dt}(L)}{L}$
- compute σ^{t+dt} using Eq. (40)
- compute ε_0^{t+dt}, ε_i^{t+dt} and Y^{t+dt} using the discretized constitutive laws
- update the mechanical fields: $\sigma^t \leftarrow \sigma^{t+dt}$; $\varepsilon_0^t \leftarrow \varepsilon_0^{t+dt}$; $\varepsilon_i^t \leftarrow \varepsilon_i^{t+dt}$

}

---------- (Viscoelastic damage phase) ----------

time initialization: $t_n \leftarrow t$

initialization of the damage front location : $l^{t_n} = 0$

discretization of length l_c into N_x elements of size dx

while $l_{t_n} < l_c$ and $dt_n > 0$ {

- advance the damage front location $l^{t_n+dt_n} = l^{t_n} + dx$ and compute $D^{t_n+dt_n}$
- $dt_n^k = 0$

while $\left|\bar{f}\left(t_n + dt_n^k\right)\right| > \epsilon$ {

- compute $\bar{f}'\left(t_n + dt_n^k; \mathcal{S}_n\right) = \left[\bar{f}\left(t_n + dt_n^k + \delta t_\epsilon; \mathcal{S}_n\right) - \bar{f}\left(t_n + dt_n^k; \mathcal{S}_n\right)\right]/\delta t_\epsilon$
- compute $\delta t^k = -\bar{f}\left(t_n + dt_n^k; \mathcal{S}_n\right) / \bar{f}'\left(t_n + dt_n^k; \mathcal{S}_n\right)$
- $dt_n^k \leftarrow dt_n^k + \delta t^k$

}

- $dt_n \leftarrow dt_n^k$
- compute $\sigma^{t_n+dt_n}$ using Eq. (43)
- compute the mechanical state in $t_n + dt_n$ in the damaged and undamaged zones using the discretized constitutive laws → $\mathcal{S}_{n+1}$
- update the mechanical fields in the damaged and undamaged zones : $\mathcal{S}_n \leftarrow \mathcal{S}_{n+1}$
- $t_n \leftarrow t_n + dt_n$

}

Remark: at the end of the pure viscoelastic phase, Newton's iterations are also performed to compute the exact time corresponding to $Y = Y_c$

Fig. 7. Diagram summary of the implemented algorithm

4. Numerical example: simulation of Uniaxial Tensile Stress Tests (UTST) at different temperatures

A first evaluation of the capability of the DGKV-TLS model to simulate the viscoelastic damage behavior of asphalt concrete (AC) is now presented. This assessment accomplished by comparing the model to uniaxial tensile stress tests performed on AC at a constant deformation rate and for four different temperatures. The (reversible) thermo-sensitive viscoelastic behavior of the AC material was first characterized by complex modulus tests carried out in the laboratory.

4.1 Characterization of the viscoelastic behavior of the AC material

A usual campaign of complex modulus tests was previously performed at University Gustave Eiffel [26] to characterize the reversible behavior of the AC material (medium coarse asphalt 0/14). This campaign was performed for cross conditions of temperature and frequency. The test results were used to calibrate the viscoelastic part of the model (the Huet model and subsequently the GKV model) and the coefficients of the Williams-Landel-Ferry (WLF) law [27]. Eleven Kelvin-Voigt units were necessary to obtain a correct fit of the Huet model. The back-calculated parameter values are listed in Table 1 and 2.

KV unit	E_i(MPa)	$\tau_{i,ref}$(s) at $\theta_{ref} = 20°C$
0	31770	N/A
1	87398	10^{-5}
2	123414	10^{-4}
3	65830	10^{-3}
4	62457	5.10^{-3}
5	62661	10^{-2}
6	7305	10^{-1}
7	12500	1
8	418	10^{1}
9	1743	10^{2}
10	79	5.10^{2}
11	39	10^{3}

Table 1. Parameter values for the GKV model

θ_{ref} (°C)	C_1	C_2 (°C)
20	29.095	211.60

Table 2. Coefficients of the WLF law given by: $a_T(T) = 10^{-C_1(\theta-\theta_{ref})/(C_2+\theta-\theta_{ref})}$

As an illustration, Fig. 8 shows the comparison between the experimental master curve plotted for θ_{ref} and that resulting from the calibrated GKV model.

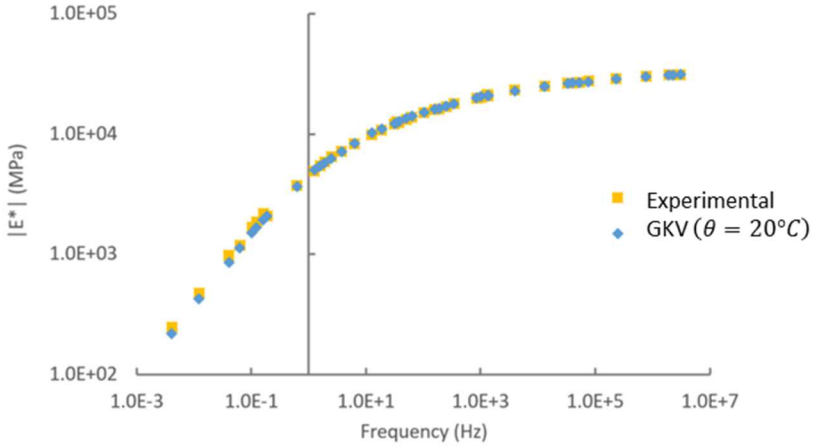

Fig. 8. Experimental master curve and calibrated GKV response

4.2 Simulations of UTST with the viscoelastic TLS model (DGKV-TLS)

The AC material described above was used to perform UTST tests on cylindrical specimens 16 cm high and 5 cm in diameter. The tests were carried out at the constant displacement rate of $1.6\ 10^{-5}\ m/s$ (mean strain rate of $10^{-4}\ s^{-1}$) and for four temperatures: $-20°C$, $-10°C$, $5°C$ and $20°C$. The tests were repeated two or three times for each temperature. The force-displacement curves were recorded until rupture occurred.

The developed program that implements the DGKV-TLS model was used to simulate these tests using the same material parameter values for the different temperatures, except for the critical energy release rate, Y_c, which was chosen as a function of T. Consistent with the literature, l_c was chosen equal to 4.5 cm corresponding to about three times the maximum grain size of the AC material. The other parameters including $Y_c(T)$ (Fig. 9) were determined to yield a correct comparison with the overall experimental results. The thermal sensitivity of Y_c found here can be compared to other research from the literature that also mentioned the dependency of the fracture properties of AC materials to temperature [28]–[30]. In this last reference for example, the experimental stress-strain response of semi-circular beam fracture tests (SCB) performed at different temperatures and loading rates were well fitted by using a cohesive zone model (CZM) whose fracture energy was function of temperature in the same way as shown Fig. 9 for $Y_c(T)$.

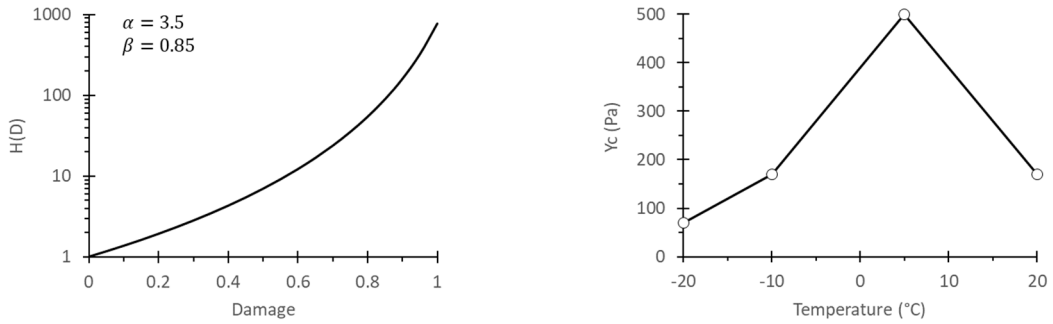

Fig. 9. (Left) evolution of the softening function $H(D)$ with damage for $\alpha = 3.5$ and $\beta = 0.85$, (Right) evolution of Y_c with temperature

The simulations were performed considering a constant increment step of the damage front equal to $l_c/100$. The timestep during the purely viscous phase could be chosen quite large as compared to the smallest response time $\tau_i(T)$ of the viscoelastic discrete spectrum thanks to the implicit scheme of time discretization.

Fig. 10a shows the UTST results and the comparison with the simulation. The experimental results are presented for four temperatures and two repetitions of the tests for each of them. These exhibit a strong effect of temperature on the evolution of the stress and the mean strain until rupture that occurs abruptly at the end of the curves in this figure.

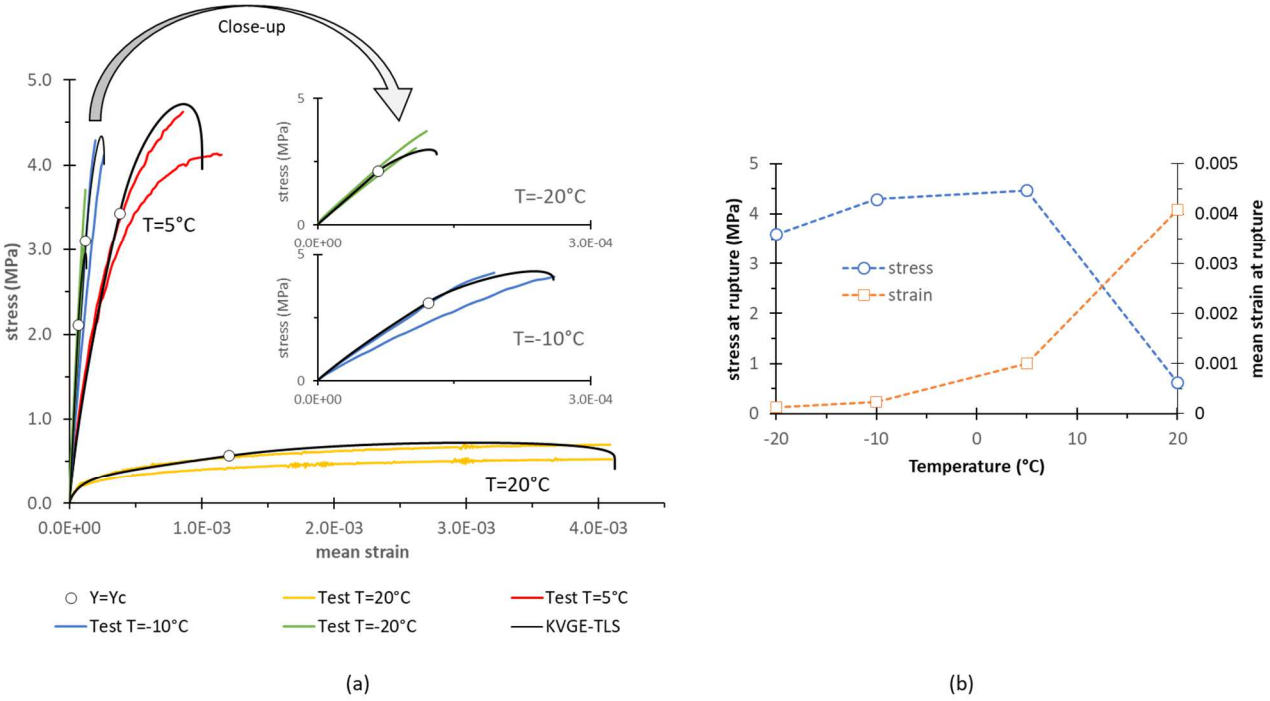

(a) (b)

Fig. 10. (a) Comparison between the experimental UTST stress-mean strain curves and those obtained using the DGKV-TLS model. Two test results are presented for each temperature. Abrupt rupture occurs at the end of these experimental and numerical curves. (b) Experimental stress and mean strain at rupture versus temperature.

As shown in Fig. 10b, the mean strain at rupture increases monotonously with temperature whereas the stress at rupture increases slightly with temperature from -20°C to 5°C prior to significantly drop. This was already reported in the literature (*e.g.* [31], [32]). The numerical simulations show a fair agreement with the overall test data. The white dots in Fig. 10a indicate the initialization of damage ($Y = Y_c$) corresponding to the transition between the pure viscoelastic phase occurring at the beginning and the viscoelastic damage phase. One can notice that this transition is smooth in the model and does not highlight any specific change of trend in the evolution that could be noticed experimentally under monotonic loading. The relative location of this transition with respect to the mean deformation at rupture is found to decrease with temperature. The damage phase lasts approximately for 50% of the simulation at $T = -20°C$ and more than 70% at $T = 20°C$.

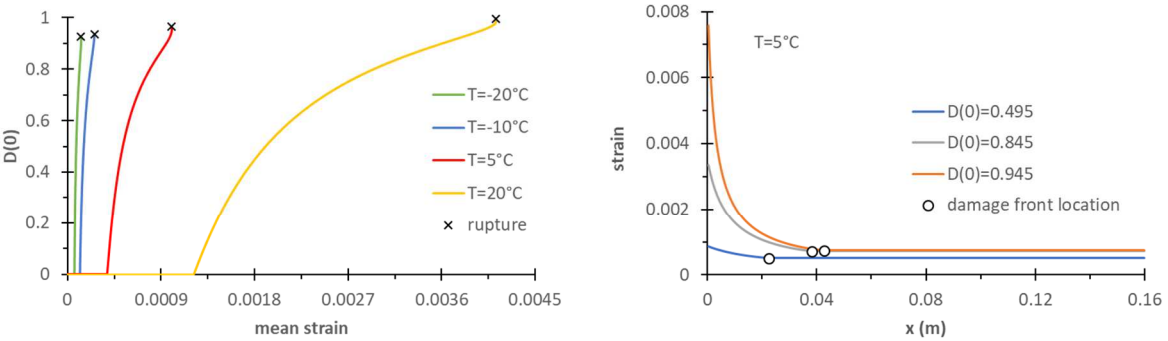

(a) (b)

Fig. 11. (a) Evolution of damage computed at the clamped end of the bar ($x = 0$) versus mean strain for the different temperatures. (b) Strain profile along the bar for several locations of the damage front at $T = 5°C$.

Fig. 11a shows, for the different temperatures, the evolution of the numerical damage computed in $x = 0$ which at any time is the maximum value of damage reached within the damaged zone. As a reminder, the damage

profile dictated by the choice of $D(\varphi)$ is linear over the interval $x \in [0, l(t)]$ with $D\big(l(t)\big) = 0$. The pure viscoelastic phase and the viscoelastic damage phase can be noticed in this figure too as well as their relative duration. Fig. 11b illustrates strain profiles along the bar computed for $T = 5°C$ and at different stages of damage growth. As expected, high strain values are obtained in the damage area as compared to those in the healthy material. These values justify the level of stress at rupture despite the high maximum values of damage reached in x=0 which are between 0.9 and 1 for the four temperatures.

4.3 Additional discussion

4.3.1 Atypical experimental result obtained for $T = 5°C$

One of the three tests performed at 5°C led to the atypical stress-mean strain curve shown in Fig. 12a, exhibiting a decrease of the stress after the peak and a high value of mean strain at rupture. This type of response was observed only in this case among all the other tested temperatures. Nevertheless, this could result from a more distributed damage along the bar. Considering this assumption, a way to simulate such response with the TLS approach is to increase the value of the critical length, l_c, what tends to uniformize the damage along the bar. Another way consists in increasing the number of damage triggers along the bar. For the 1D problem considered here, it can be shown that this is equivalent to affect l_c with the maximum cumulated damageable length resulting from these triggers when considering similar non-overlapping bands growing at the same rate (Fig. 12).

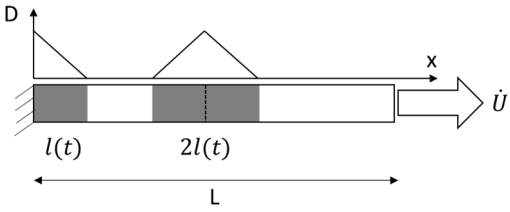

Fig. 12. TLS modeling of the bar considering two damage triggers: one of maximum length l_c located at the clamped end and the other one of maximum length $2l_c$ centered at some point in $x > 2l_c$ (equivalent to the previous simulation described in Fig. 5, substituting l_c by $3l_c$).

Fig. 13a shows an example of computation carried out for a critical length equal to five times the previous value. As shown in this figure, the TLS stress-mean strain curve thus obtained leads to a longer damage phase which induces an increase of the mean strain at rupture and to an evolution closer to the experimental atypical one. Note that the higher l_c, the closer the TLS curve to that of the local response given by the constitutive law of Fig. 4. Superimposition is obtained for sufficiently large values of l_c (Fig. 13b).

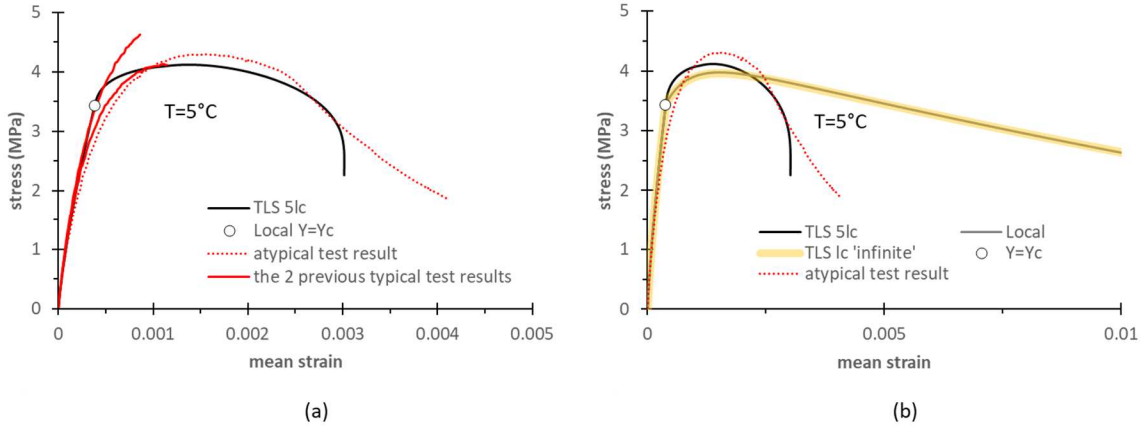

Fig. 13. (a) Atypical test result obtained for $T = 5°C$ and comparison with the typical results and the TLS simulations with l_c equal to five times its initial value, (b) Comparison with the response given by the local constitutive law.

4.3.2 Comparison between the TLS in viscoelasticity and in elasticity using an equivalent secant modulus

Comparisons with TLS computations in elasticity were performed to explore the possibility of simplifying the viscoelastic approach. These were done considering a Young modulus as a function of temperature and equal to the secant modulus of the viscoelastic curves at point $Y = Y_c$ (initiation of damage). Fig. 14 shows that, as expected, a good agreement can be obtained at low temperatures. However, a significant difference is observed at higher temperatures, especially in terms of the value of the mean strain at rupture, implying the need for using viscoelasticity in general.

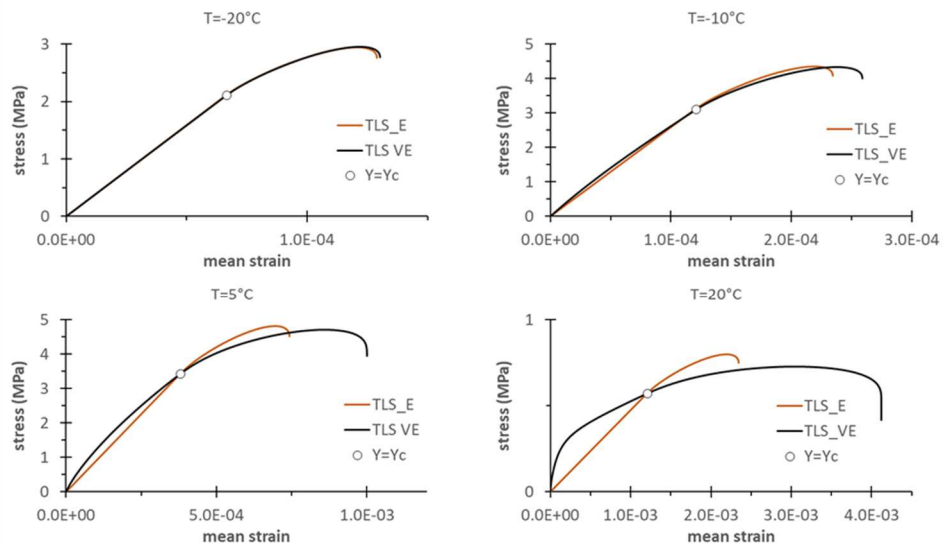

Fig. 14. Comparison of the TLS stress-mean strain curves obtained in elasticity and viscoelasticity

4.3.3 Energetic aspect of the bar response computed with the viscoelastic TLS approach

The viscoelastic TLS model can be used to investigate the different energies involved in the bar during loading until rupture. One can distinguish the total energy (FU = the work of external forces) injected into the bar, the energy dissipated by either viscoelasticity (W_{VE}) or damage (W_D) and the stored elastic energy ($FU - W_{VE} - W_D$). For a bar of unit section, these are given by:

$$FU(t) = \int_0^t \sigma(t)\dot{U}dt \tag{52}$$

$$W_{VE}(t) = \int_0^t \int_0^L \sigma_{VE}(\dot{\varepsilon} - \dot{\varepsilon}_0)\,dxdt = \int_0^t \left[\int_0^{l(t)} (1 - D(x,t)) \sum_i E_i \tau_i \dot{\varepsilon}_{i,D}^2(x,t)\,dx + (L - l(t)) \sum_i E_i \tau_i \dot{\varepsilon}_{i,ND}^2(t)\right] dt \tag{53}$$

$$W_D(t) = \int_0^t \int_0^L Y_c H(D)\dot{D}dx\,dt = \frac{Y_c(\theta) l_c}{\beta^2(\alpha-1)(\alpha-2)} \left[\frac{1}{\left(1-\frac{\beta l(t)}{l_c}\right)^{\alpha-2}} - \frac{\beta(\alpha-2)}{l_c} l(t) - 1\right] \tag{54}$$

$$W_{dissipated}(t) = W_{VE}(t) + W_D(t) \tag{55}$$

$W_{dissipated}$ denotes the total energy dissipated in the bar. FU and W_{VE} are computed numerically. The expression of W_D can be derived analytically leading to the equation above which, for a given damage front location, $l(t)$, depends on temperature because of $Y_c(T)$ only.

Fig. 15a shows these quantities computed for $T = 5°C$. In this case, the total energy dissipation is approximately half the total energy input at rupture and is composed of about 30% of damage dissipation and 70% of viscous dissipation. Fig. 15b shows the total energy input at rupture as a function of temperature. FU exhibits a maximum in $T = 5°C$ and has a similar shape as $Y_c(T)$ but without being homothetical. Fig. 15c shows that the ratio of damage dissipation over the total energy input (W_D/FU) slightly decreases with temperature. This figure

also shows that, as expected, the energy dissipation at low temperatures is mainly due to damage whereas it results mostly from viscoelasticity at higher temperatures (ratio $W_D/(W_D + W_{VE})$).

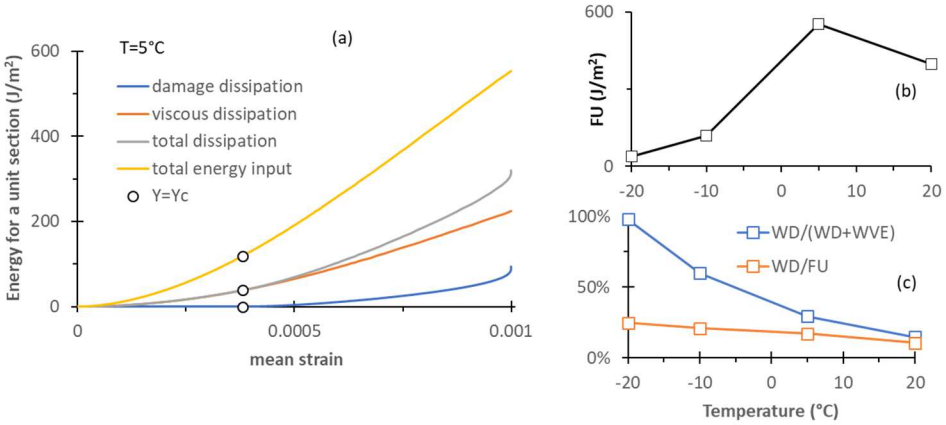

Fig. 15. Energy computation with the viscoelastic TLS model for the bar of unit section: (a) evolution of the different energies involved in the bar for $T = 5°C$, (b) total energy input (FU) at rupture versus temperature, (c) energy dissipated by damage (W_D) over either the total dissipation ($W_D + W_{VE}$) or the total energy input (FU) versus temperature.

Conclusion

The development of a 1D viscoelastic damage model relying on the thick level set (TLS) approach is presented in this paper. This model is meant to be applied to the study of bituminous materials and structures to fracture. The Generalized Kelvin-Voigt (GKV) spectral decomposition of the creep function is used to represent the pure viscoelastic initial behavior of the material whose thermo-sensitivity is accounted for through the time-temperature superposition principle. Damage is introduced at the local scale based on the effective stress principle. Further for structural applications, the TLS approach is utilized to regularize the damage evolution law postulated at the local scale. For the first time, this novel model extends the TLS approach to viscoelasticity.

The developed model is applied to the analysis of uniaxial tension stress tests (UTST) performed in the laboratory on asphalt concrete at different temperatures and for the same imposed displacement rate. The experimental force-displacement curves obtained are much different depending on the test temperature reflecting either fragileness or ductileness of the specimens. Making the critical energy release rate (Y_c) depend on temperature, a good match between the experimental and the numerical results can be obtained for all the tested conditions proving the capability of the model to simulate fracture processes in bituminous materials under monotonic loading. In contrast, the test results could not be reproduced by similar TLS simulations but performed in elasticity, even trying to determine the Young modulus as a function of temperature. Interestingly, the energy dissipated by viscosity and damage can be easily derived from the developed model. In the simulations presented in this paper, the dissipation for $T < -20°C$ is almost due to damage only whereas it is mainly due to viscosity for $T > 20°C$.

The next step to this research will be to assess the predictive nature of the model in 1D or to adapt the choice of the damage parameters (functions $H(D), Y_c(T)$ ~~and possibly $l_c(T)$~~). This will require to carry out additional tests for a wider set of experimental conditions, in particular varying the displacement rate. An effort will also be made to better characterize the development of one or more damage bands. To address more general test geometry, the implementation of the model in 2D will be achieved.

References

[1] M. L. Williams, "Initiation and Growth of Viscoelastic Fracture," *Int. J. Fract. Mech.*, 1965, doi: 10.1007/bf03545561.

[2] L. J. Bonis and J. J. Duga, "Fundamental Phenomena in the Materials Sciences," *Science (80-.).*, vol. 155, no. 3760, pp. 357–361, Jan. 1967, doi: 10.1126/science.155.3760.357.

[3] W. G. Buttlar, A. Chabot, E. V. Dave, C. Petit, and G. Tebaldi, "Mechanisms of Cracking and Debonding in Asphalt and Composite Pavements," *RILEM State-of-the-Art Reports*. 2018.

[4] X. Li and M. O. Marasteanu, "Investigation of Low Temperature Cracking in Asphalt Mixtures by Acoustic Emission," *Road Mater. Pavement Des.*, 2006, doi: 10.1080/14680629.2006.9690048.

[5] Y. S. Jeng and J. D. Perng, "Analysis of Crack Propagation in Asphalt Concrete Using Cohesive Crack Model YEOU-SHANG }ENQ

AND }IA-DER PERNG," *Transp. Res. Rec. 1317, 90–99*, no. 3, 1991.
[6] Y. S. Jeng, C. Liaw, and P. Liu, "Analysis of crack resistance of asphalt concrete overlays – a fracture mechanics approach," *Transp. Res. Rec. 1388, 160–166*, 1993.
[7] Y. R. Kim, "Cohesive zone model to predict fracture in bituminous materials and asphaltic pavements: State-of-the-art review," *International Journal of Pavement Engineering*. 2011, doi: 10.1080/10298436.2011.575138.
[8] S. H. Song, G. H. Paulino, and W. G. Buttlar, "A bilinear cohesive zone model tailored for fracture of asphalt concrete considering viscoelastic bulk material," *Eng. Fract. Mech.*, 2006, doi: 10.1016/j.engfracmech.2006.04.030.
[9] F. T. S. Aragão, Y.-R. Kim, and M. H. Javaherian, "Modeling Rate-dependent Fracture Behavior of Asphalt Mixtures," *Pap. Submitt. to Transp. Res. Board*, 2012.
[10] N. Moës and T. Belytschko, "Extended finite element method for cohesive crack growth," *Eng. Fract. Mech.*, 2002, doi: 10.1016/S0013-7944(01)00128-X.
[11] V. B. Pandey, I. V. Singh, B. K. Mishra, S. Ahmad, A. V. Rao, and V. Kumar, "Creep crack simulations using continuum damage mechanics and extended finite element method," *Int. J. Damage Mech.*, 2019, doi: 10.1177/1056789517737593.
[12] H. H. Zhang, G. Rong, and L. X. Li, "Numerical study on deformations in a cracked viscoelastic body with the extended finite element method," *Eng. Anal. Bound. Elem.*, 2010, doi: 10.1016/j.enganabound.2010.02.001.
[13] G. Pijaudier-Cabot and Z. P. Bazant, "Nonlocal Damage Theory," *J. Eng. Mech.*, vol. 113, no. 10, pp. 1512–1533, 1987, doi: 10.1061/(ASCE)0733-9399(1987)113.
[14] D. Bodin, G. Pijaudier-cabot, C. D. La Roche, J. Piau, and A. Chabot, "Continuum Damage Approach to Asphalt Concrete Fatigue Modelling To cite this version : Continuum Damage Approach to Asphalt Concrete Fatigue Modeling," *J. Eng. Mech.*, pp. 0–9, 2004.
[15] R. H. J. Peerlings, R. De Borst, W. A. M. Brekelmans, and J. H. P. De Vree, "Gradient enhanced damage for quasi-brittle materials," *Int. J. Numer. Methods Eng.*, vol. 39, no. 19, pp. 3391–3403, Oct. 1996, doi: 10.1002/(SICI)1097-0207(19961015)39:19<3391::AID-NME7>3.0.CO;2-D.
[16] A. Karma, D. A. Kessler, and H. Levine, "Phase-field model of mode III dynamic fracture," *Phys. Rev. Lett.*, vol. 87, no. 4, pp. 45501-1-45501–4, 2001, doi: 10.1103/PhysRevLett.87.045501.
[17] R. Shen, H. Waisman, and L. Guo, "Fracture of viscoelastic solids modeled with a modified phase field method," *Comput. Methods Appl. Mech. Eng.*, 2019, doi: 10.1016/j.cma.2018.09.018.
[18] N. Moës, C. Stolz, P. E. Bernard, and N. Chevaugeon, "A level set based model for damage growth: The thick level set approach," *Int. J. Numer. Methods Eng.*, 2011, doi: 10.1002/nme.3069.
[19] C. Stolz and N. Moës, "A new model of damage: A moving thick layer approach," *Int. J. Fract.*, vol. 174, no. 1, pp. 49–60, 2012, doi: 10.1007/s10704-012-9693-3.
[20] A. Salzman, N. Moës, and N. Chevaugeon, "On use of the thick level set method in 3D quasi-static crack simulation of quasi-brittle material," *Int. J. Fract.*, vol. 202, no. 1, pp. 21–49, 2016, doi: 10.1007/s10704-016-0132-8.
[21] C. Huet, "Etude par une méthode d'impédance du comportement viscoélastique des matériaux hydrocarbonés," *Thèse Docteur Ingénieur, Fac. des Sci. l'Université Paris*, 1963.
[22] C. Huet, "Coupled size and boundary-condition effects in viscoelastic heterogeneous and composite bodies," *Mech. Mater.*, vol. 31, no. 12, pp. 787–829, 1999, doi: 10.1016/S0167-6636(99)00038-1.
[23] S. P. C. Marques and G. J. Creus, *Computational Viscoelasticity*, no. 9783642253102. Berlin, Heidelberg: Springer Berlin Heidelberg, 2012.
[24] H. W. Kuhn and A. W. Tucker, "non-linear programming," in *The New Palgrave Dictionary of Economics*, no. x, Berkeley, Calif.: University of California Press, 1951, pp. 481–492.
[25] L. A. T. Mororó and F. P. van der Meer, "Combining the thick level set method with plasticity," *Eur. J. Mech. A/Solids*, vol. 79, no. April 2019, p. 103857, 2020, doi: 10.1016/j.euromechsol.2019.103857.
[26] V. T. Vu, "Etude expérimentale et numérique du comportement au gel et au dégel des enrobés bitumineux partiellement saturés," Thesis (PhD), Ecole Centrale Nantes, France, 2017.
[27] M. L. Williams, R. F. Landel, and J. D. Ferry, "The Temperature Dependence of Relaxation Mechanisms in Amorphous Polymers and Other Glass-forming Liquids," *J. Am. Chem. Soc.*, vol. 77, no. 14, pp. 3701–3707, Jul. 1955, doi: 10.1021/ja01619a008.
[28] M. Fakhri, E. Haghighat Kharrazi, M. R. M. Aliha, and F. Berto, "The effect of loading rate on fracture energy of asphalt mixture at intermediate temperatures and under different loading modes," *Frat. ed Integrita Strutt.*, 2018, doi: 10.3221/IGF-ESIS.43.09.
[29] F. T. S. Aragão, Y.-R. Kim, and M. H. Javaherian, "Modeling Rate-dependent Fracture Behavior of Asphalt Mixtures," *Pap. Submitt. to Transp. Res. Board*, no. July 2011, pp. 1–17, 2012.
[30] S. Im, Y. R. Kim, and H. Ban, "Rate- and temperature-dependent fracture characteristics of asphaltic paving mixtures," *J. Test. Eval.*, 2013, doi: 10.1520/JTE20120174.
[31] A. F. Stock and W. ARAND, "Low temperature cracking in polymer modified binders," *J. Assoc. Asph. Paving Technol.*, 1993.
[32] F. Olard, H. Di Benedetto, A. Dony, and J. C. Vaniscote, "Properties of bituminous mixtures at low temperatures and relations with binder characteristics," *Mater. Struct. Constr.*, 2005, doi: 10.1617/14132.